THF cleaning for PMMA residue removal from graphene

Master's Thesis, 1.8.2024

Author:

Sirkka Suutari

Supervisor:

Andreas Johansson

UNIVERSITY OF JYVÄSKYLÄ
DEPARTMENT OF PHYSICS

Tiivistelmä

Suutari, Sirkka
PMMA-jäänteiden puhdistus grafeenista tetrahydrofuraanilla
Pro Gradu -tutkielma
Fysiikan laitos, Jyväskylän yliopisto, 2024, 45 sivua

Tutkielmassa selvitettiin tetrahydrofuraanin soveltumista grafeenin puhdistukseen kemiallisen kaasufaasipinnoituksen jälkeisestä siirtoprosessista jäävistä PMMA-tukikerroksen jäänteistä, sekä sen soveltuvuutta pintadouppauksen poistoon. Piidioksidi-substraatille grafeenista valmistettujen Hall bar -laitteiden sähköiset ominaisuudet kartoitettiin puhdistuksen eri vaiheissa. Pintadouppauksen määrää ja grafeenin laatua arvioitiin käyttämällä Raman-spektroskopiaa ja PMMA-jäänteiden määrää seurattiin atomivoimamikroskopialla. Sähköiset mittaukset ja Raman-spektroskopia osoittivat tutkittujen laitteiden olevan ennen puhdistusta voimakkaasti p-doupattuja ja näyttivät douppauksen vähentyneen puhdistuksen jälkeen. Tutkittu puhdistusprosessin sopivuudesta PMMA jäänteiden poistoon ei saatu ratkaisevaa tulosta, mutta se osoitti lupausta muun pintadouppauksen poistossa.

Avainsanat: grafeeni, tetrahydrofuraani, PMMA, kemiallinen kaasufaasipinnoitus

Abstract

Suutari, Sirkka
THF cleaning for PMMA residue removal from graphene
Master's thesis
Department of Physics, University of Jyväskylä, 2024, 45 pages.

In this work the effectiveness on tetrahydrofuran cleaning on PMMA residues left behind from the polymer supported transfer process of CVD grown graphene and its ability to remove surface doping from graphene were studied. The electronic properties of the studied graphene Hall bar devices fabricated on a silicon dioxide substrate were charted during different points of the cleaning process. The amount of surface doping and the quality of the graphene was estimated using Raman spectroscopy and the amount of PMMA residues was estimated using atomic force microscopy. The electrical measurements and Raman spectroscopy showed that before cleaning the devices were highly p-doped and that the doping was reduced as a result of the cleaning. The suitability studied cleaning process for PMMA residue removal could not be conclusively estimated from the obtained results, but the process showed promise for removing ambient surface doping.

Keywords: graphene, tetrahydrofuran, PMMA, chemical vapor deposition

Contents

1 Introduction

The demand for small, complex technology is constantly growing and it is being answered by nanoscale solutions as new attractive properties in nanomaterials and their possible applications are discovered. Nanomaterials, such as nanoparticles and one- and two-dimensional materials, offer novel properties compared to the same materials in bulk. 2D materials, which can be as thin as a single layer of atoms, have many advantages - they have a large surface area compared to their mass, the confinement of electrons into two dimensions brings about unique electronic properties [1], and high exposure of surface atoms allows for relatively easy modulation of properties [2].

Graphene was the first of many 2D materials to be discovered. It is found in nature in graphite, which consist of stacked graphene layers weakly adhered to each other via van der Waals forces. Small flakes of graphene were first isolated from graphite in 2004 by exfoliation with ordinary tape [3]. Thanks to its wide range of special properties graphene has since become one of the favourites of nanomaterials research alongside nanoparticles and nanotubes, holding fast even as new 2D materials emerge. Graphene is a one-atom thick sheet formed of carbon atoms in a honeycomb structure, held together by strong in-plane covalent bonds. Graphene's structure brings about high tensile strength [4], flexibility [4], good carrier mobility [3] and transparency. Its unique properties make it suitable for challenging applications such as medical devices [5] or high-frequency electronics [6].

Graphene's properties can be further modified when needed - for example by chemical functionalization [7], introducing defects [8] or strain [9] or by modifying the third dimension of graphene, such as with optical forging [10]. Since graphene is all surface, these modifications are relatively easy to make. On the flip side of easy modification, the same properties leave graphene prone to unwanted effects on its properties caused by impurities. These impurities can be reduced to a degree by adjusting the methods of graphene synthesis and device fabrication [11]. The most commonly used synthesis method is decidedly chemical vapor deposition CVD, since it can be used to produce large graphene sheets of relatively good quality [12][13].

CVD in itself produces relatively good quality graphene, but further use of graphene produced with it requires a polymer supported transfer process [14][15] that can compromise the quality and leave behind contamination from the supporting polymer layer [16].

Whereas synthesis methods such as mechanical exfoliation might produce graphene of considerably better quality, they fall short of the demands for scale and reliability [13]. As contamination during synthesis, device fabrication and storage cannot be completely eliminated, ways to clean graphene are needed regardless of development in the aforementioned steps. The goal of the work presented in this thesis was to estimate the effectiveness of using tetrahydrofuran, a polar solvent commonly used for polymers, for cleaning polymer residue and removing surface doping from graphene.

2 Graphene

Even before its discovery in 2004, graphene had been known for a long time as a purely theoretical material. The first paper describing the band structure of graphene for example was published in 1947, where P.R. Wallace used it as a starting point for describing the band structure of graphite[17]. The discovery of a real graphene sample, and its reported properties resulted in a proverbial goldrush into graphene research that has only levelled out in recent years. In the 20 years of active research into applications, a plethora of possible use cases for graphene have been proposed but realised products are still few and far between. Part of this is due to graphene research being a relatively young field, but another barrier is the scalable production of high quality graphene films. This has in part been answered by the synthesis of graphene by chemical vapor deposition, but it is not without its drawbacks. This chapter will first introduce the relevant properties of graphene and then illustrate the challenges of achieving a clean final product when synthesising graphene with CVD.

2.1 Graphene's structure and electronic properties

Graphene is an atomically thin material consisting of sp^2 hybridized carbon atoms arranged in a honeycomb structure, as shown in figure 1. It is commonly found in nature as the fundamental building block of graphite, which consists of graphene layers held together by van der Waals interaction. Besides the three-dimensional graphite, graphene is also the parent structure of one-dimensional nanotubes and zero-dimensional fullerenes. Carbon has four valence electrons in the configuration [He]$2s^2 2p^2$. In sp^2 hybridized carbon three of those electrons populate the sp^2 orbitals, leaving one electron for the p_z orbital. The overlapping sp^2 orbitals couple to form σ-bonds, the remaining p_z orbitals forming the half-filled π bands responsible for the electronic properties of graphene. The σ-bonds are very strong and give graphene its high mechanical strength and stiffness, a tensile strength of 130 GPa and a Young's modulus of 1 TPa [4] respectively. Besides explaining graphene's excellent mechanical strength, the sp^2 hybridization results in the 120° angle between the bonds and so

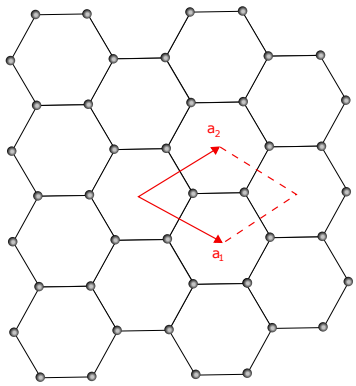

Figure 1. Graphene lattice consists of carbon atoms arranged in a honeycomb lattice. Graphene's unit cell contains two atoms and is defined by vectors a_1 and a_2. Most of graphene's interesting properties arise from its highly ordered structure and one-atom-thickness.

the formation of the honeycomb lattice.

In addition to being very strong despite its thinness, thanks to the sp^2 hybridization, graphene is an excellent conductor of electricity and heat. Assuming the electrons forming the co-planar σ-bonds, do not play a part in conductivity and limiting electron hopping to nearest and next to nearest neighbours, the tight binding approach can be used to calculate graphene's dispersion relation [17][18]

$$E(\vec{k}) = \pm t\sqrt{3 + f(\vec{k})} + t' f(\vec{k}), \tag{1}$$

where $t \approx 2.8$ eV is the nearest-neighbour hopping energy and t' is the next nearest-neighbour hopping energy and $\vec{k}$ is the position in momentum space. The next nearest-neighbour hopping energy t' is small compared to the nearest-neighbour one [18]. The function $f(\vec{k})$ is defined as

$$f(\vec{k}) = 2\cos\left(\sqrt{3}k_y a\right) + 4\cos\left(\frac{\sqrt{3}}{2}k_y a\right)\cos\left(\frac{3}{2}k_x a\right), \tag{2}$$

where a is the lattice constant. The points at the corners of graphene's first Brillouin zone, where the π bands touch, are called the Dirac points. These points in the momentum space are described by the vectors

$$\vec{K} = \left(\frac{2\pi}{3a}, \frac{2\pi}{3\sqrt{3}a}\right), \qquad \vec{K'} = \left(\frac{2\pi}{3a}, -\frac{2\pi}{3\sqrt{3}a}\right). \tag{3}$$

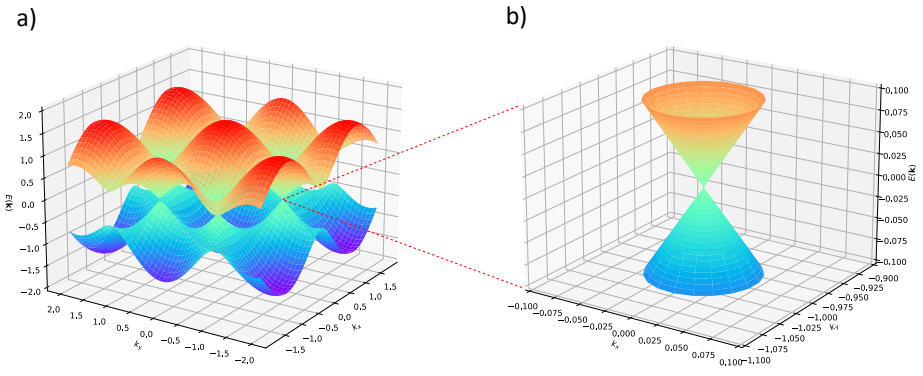

Figure 2. a) Graphene's dispersion relation in the 1st Brillouin zone. Graphene has no band gap, so it is called a zero-gap semiconductor or a semimetal. b) Graphene's dispersion for low energies is linear. At E(k)=0 we see the Dirac point. Arbitrary units.

If we expand equation 2 close to the Dirac point $\vec{K}$, for $\vec{k} = \vec{K}+\vec{q}$, where $||\vec{q}|| << ||\vec{K}||$ ignoring t' since it is small, we get $f(\vec{q}) \approx \frac{9a^2}{4}(q_x^2 + q_y^2) - 3$. So for low energies near the Dirac points the energy dispersion relation is

$$E(\vec{q}) = \pm\frac{3ta}{2}||\vec{q}|| = \pm v_F||\vec{q}||. \tag{4}$$

The dispersion relation in the 1st Brillouin zone and the linear dispersion relation for low energies is visualised in figure 2. The behaviour of electrons in graphene differs from that of conventional semiconductors, where the dispersion relation is commonly quadratic near the band gap. Single layer graphene has no band gap, so graphene is often called a zero-gap semiconductor, as there is no forbidden region between the valence and conduction band, but the density of states vanishes at the Dirac point for pristine graphene. In non-pristine 'real' graphene point defects cause the density of states at the Dirac point to become finite [19]. The low density of states makes graphene sensitive to changes near the Dirac point.

Graphene's conduction can also be externally controlled by gating, meaning its charge carriers can be continuously tuned between holes and electrons [3] as shown in figure 3. The charge neutrality point where graphene reaches maximum resistance

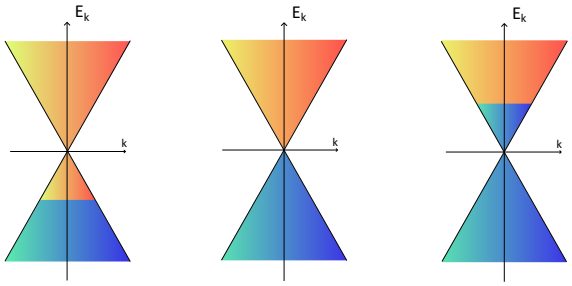

Figure 3. Graphene's charge carriers can be tuned between holes (orange) and electrons (blue) by using a gate voltage or by doping. The left Dirac cone's Fermi level is below the Dirac point, corresponding to holes populating the valence band and the right cone's Fermi level is above the Dirac point, corresponding to electrons populating the conduction band. The middle cone represents the neutral situation.

is called the Dirac point. In pristine graphene the Fermi level lies at the Dirac point, but in doped graphene it shifts away from the Dirac point as the material gathers an excess of electrons or holes. The Dirac point of doped graphene can be reached by tuning the carriers using external gating.

Some of graphene's properties, such as high thermal and electrical conductance suffer as defects are introduced. Despite this, defects can also be desirable as they can be used to control graphene's properties. Dangling bonds from graphene defects can also form bonds with impurity atoms or molecules. Defects in graphene can be formed in a few main ways: during crystal growth, such as when domains growing from different nucleation points meet in CVD, chemical methods and irradiation. Defects can be used to functionalize graphene, add metallic contacts, open a bandgap or induce curvature. Beyond the degradation of properties caused by defects graphene in real applications is also affected by the substrate it is deposited on. The mobility of graphene suffers as graphene is transferred onto SiO_2 due to impurity scattering [20]. The effect of the substrate is made clear by the considerably improved mobilities reported for suspended graphene devices [21].

2.2 Clean graphene

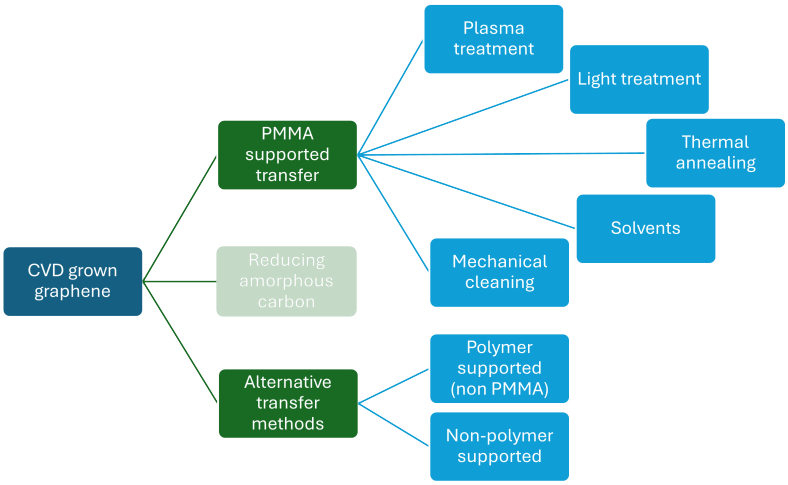

Figure 4. A variety of approaches have been studied in the chase for cleaner CVD grown graphene. The recognised problem of PMMA residues has been approached in two main ways: either studying ways of cleaning graphene or eliminating PMMA from the transfer process altogether. Separately, the contamination from amorphous carbon and its link to PMMA residues have been studied.

Among the number of methods for fabricating graphene, chemical vapor deposition CVD is comparatively low cost and high quality and can be used to produce large graphene sheets. Since it was first reported [22], it has grown to be one on the most common methods for producing graphene. CVD graphene is grown on transition metal films that act as a catalyst [12]. Most applications, however, require graphene on a dielectric substrate, not a transition metal film. To use graphene produced by CVD for further application, it needs to be transferred from the metal growth surface to the desired substrate. This transfer is commonly done by coating the graphene with a polymer layer, etching away the metal film, then transferring the polymer supported graphene onto the target substrate and finally removing the polymer with a solvent and annealing, ideally leaving behind just the graphene on the desired substrate. This process is illustrated in figure 5.

Unfortunately, this transfer process leaves behind some polymer residue on the graphene surface. These residues, like any surface contamination in graphene, are undesirable as they disturb graphene's intrinsic properties, worsening device performance. PMMA residues cause p-type doping and bring about an increase in carrier scattering, lowering the charge carrier mobility of graphene [23]. The array of

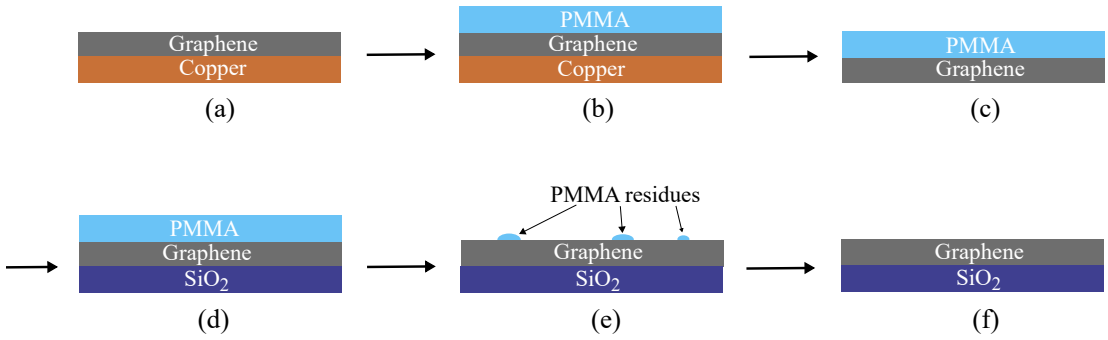

Figure 5. Schematic of the PMMA supported graphene transfer process. **a)** Graphene is first grown onto a copper film with CVD **b)** the copper-graphene stack is spin coated with PMMA **c)** the copper film is etched away **d)** the PMMA supported graphene is rinsed clean of remaining etchant and captured onto the desired substrate, most commonly SiO_2, **e)** after the PMMA supported graphene is captured onto the substrate and dried, the PMMA is removed, typically with acetone. This removes the bulk of the PMMA but leaves behind some hard to remove residues. **f)** With additional cleaning steps, such as annealing, we are ideally left with clean graphene on the desired substrate.

approaches for PMMA residue free graphene is presented in figure 4.

PMMA is widely used, because it is relatively cheap, has good mechanical properties, is easy to spin coat onto graphene, and is a high-resolution electron beam resist. The amount of PMMA residues can be reduced by using a PMMA with a lower average molecular weight [24]. To assure the support layer has sufficient mechanical strength, two layers of PMMA can be used: a lower molecular weight PMMA on the graphene surface and a higher molecular weight on top. Different transfer methods can be chosen to reduce the amount of residues, such as thermal release tape or different support layers. The novel transfer supports can be divided into other polymers such as parylene [25] and polystyrene [26] or non-polymer support layers such as paraffin [27] or rosin [28]. Especially paraffin as a transfer medium is promising due to its dual functionality of acting as a support during transfer and

reducing the amount of wrinkles in graphene. Naturally other graphene production methods such as mechanical or chemical exfoliation can be used to avoid the transfer residue problem altogether, but each has its own limitations and none compare to the scale and reliability that CVD provides.

Outside of sample preparation graphene is also susceptible to ambient pollution from surface adsorbates, because of its large surface to volume ratio, and contamination from amorphous carbon. Graphene can adsorb molecules such as O^2, H^2 and H_2O from ambient air, that cause surface transfer doping [29][30]. The most prominent adsobrant in ambient conditions being water molecules, measuring relative humidity when reporting electronic properties sensitive to surface adsorbates is good practice [31]. The doping from surface adsorbates is usually undesired, but its pronounced effect on graphene's electronic properties can also be used for sensitive gas sensors[32]. Graphene can also be contaminated by amorphous carbon, that can form for instance during CVD growth or as a result of some cleaning methods such as annealing [16]. Amorphous carbon contamination in itself hinders graphene's properties, but it has also been shown that eliminating amorphous carbon can reduce the amount of polymer residues left behind from the polymer supported transfer process [33].

There are a multitude of approaches that can be used to reduce the amount of PMMA residues to a minimum, such as thermal annealing, plasma or ion beam treatment [16]. Solvent rinsing is always used in some capacity as part of the generic transfer process, as acetone rinsing is usually used to remove the bulk of PMMA after the transfer. Other solvents, such as tetrahydrofuran or chloroform or can also be used to further clean the graphene surface.

Thermal annealing is done by heating the sample to a high temperature in a chosen atmosphere. The results depend on the annealing time, temperature and atmosphere. With thermal annealing there always comes a degree of reduced graphene quality in exchange for a cleaning effect[34], and higher annealing temperatures can even damage the sample substrate. Thermal annealing is often used in combination with other cleaning methods, as it alone doesn't produce satisfactory results.

Graphene can also be mechanically cleaned with an atomic force microscope (AFM) usually used for characterisation. Operating the AFM in contact mode, the tip is scanned over the sample to remove residues. Contact mode AFM cleaning has been shown to produce good cleaning results, but it demands precise control

of the used force to avoid damaging the graphene [35]. Unfortunately, the required precision makes this cleaning method hard to scale.

Plasma treatment removes PMMA residue by exposing the sample surface to plasma, that interacts with the surface. The nature of the interaction depends on the used source gas. The suitability of plasma treatment for cleaning graphene varies by method. For example H_2 inductive coupled plasma has been shown to successfully clean PMMA residue, causing little damage to the graphene, but is limited by not being suited for graphene on silicon [36]. In comparison Cl_2 plasma can be used on graphene on silicon, but has the drawback on needing more time to achieve the same cleaning result [36]. Plasma treatment can cause damage to the graphene and requires a more complicated setup.

Light treatment is a relatively gentle way of cleaning PMMA residue, preserving the quality of graphene better compared to thermal annealing and plasma treatment. Light treatments for cleaning graphene can be divided into two categories, with two different mechanisms: visible light and UV. In visible light treatment a high energy laser removes PMMA residue by laser ablation, whereas its UV counterpart causes the PMMA to degrade, weakening the interaction between it and graphene [16].

Achieving clean graphene is important not only for preserving graphene's properties, but also for ensuring reliable and repeatable conditions for studying graphene and graphene devices. Contamination can for example completely misdirect graphene sensor development [37] or hinder the modification of graphene with optical forging, leading to uneven irradiation and redeposition of PMMA.

3 Characterization methods

3.1 Raman spectroscopy

Raman spectroscopy is a non-destructive and fast characterization method, that is used to study the vibrational states of molecules, which in turn gives information about the chemical composition of a sample. Raman spectroscopy is based on inelastic scattering of photons by matter, known as Raman scattering. In Raman scattering the incident photons excite a molecule to a virtual state that in decaying re-emits a photon, returning the molecule to either a higher vibrational state, for Stokes scattering or lower, for anti-Stokes scattering. This results in the emitted photon having a shift in energy compared to the incident photon, or respectively the scattered light having a change in wavelength. The shift in photon energy gives information about the vibrational states of the molecule. In elastic Rayleigh scattering, which is much more prominent than Raman scattering, the molecule returns to the original state and the wavelength of the scattered light stays the same. In Raman spectroscopy, the sample is irradiated with laser, and the scattered light is measured and filtered to remove the elastically scattered light corresponding to the incident laser, leaving behind the Raman spectrum.

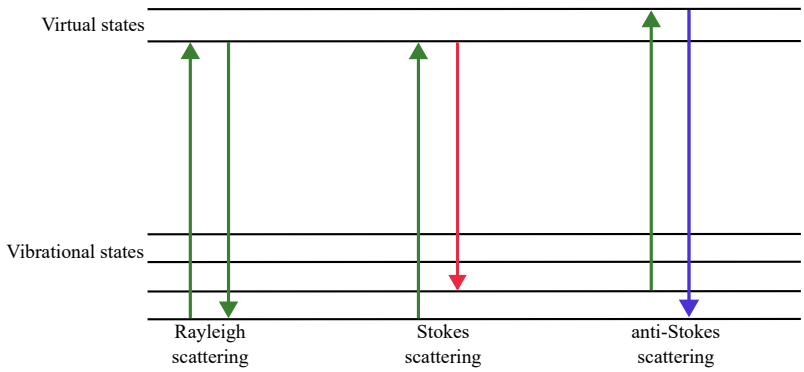

Figure 6. Raman spectroscopy is based on Raman scattering, which can be divided into Stokes scattering, where the energy of the light is shifted to a lower energy and the molecule is left on a higher vibrational state, and anti-Stokes scattering, for the opposite shift in energy. Most light scatters elastically, which is called Rayleigh scattering.

Raman spectroscopy is a particularly good tool for the characterization of graphene. The lack of a band gap means that all wavelengths of incident radiation are resonant, so in addition to the atomic structure the Raman spectrum also gives information on graphene's electronic properties [38]. The Raman spectrum of graphene has only a few prominent features, but a wealth of information can be derived from the positions, intensities and shapes of these peaks.

The Raman spectrum of graphene has three main features: the D, G and 2D peaks at around 1350 cm^{-1}, 1580 cm^{-1} and 2700 cm^{-1} respectively [39]. The positions of the peaks depend on the laser excitation energy, the cited positions for the peaks correspond to a 514 nm laser. The D peak arises from the breathing modes of the carbon rings. It is activated by defects in graphene and thus doesn't appear in pristine graphene. The G peak is due to the stretching of the σ carbon atom bonds and the 2D peak is the second order overtone of the D peak [40]. An example of a Raman spectrum for defected graphene is presented in figure 7.

The 2D peak can be used to separate single- and bi-layer graphene and graphite, since it shifts and significantly changes shape with added layers [39]. The G- and 2D-peaks can also be used to estimate the amount and nature of doping in graphene. The G peak position increases, and its width decreases for both hole and electron doping, whereas the 2D peak position increases for hole doping and decreases for electron doping. The 2D peak position is not very sensitive for small amounts of electron doping, but together with the G peak position it can still be used to determine the nature of doping [41]. The intensity of the 2D peak also decreases with doping, so the ratio I(2D)/I(G) can also be used to estimate the amount of doping.

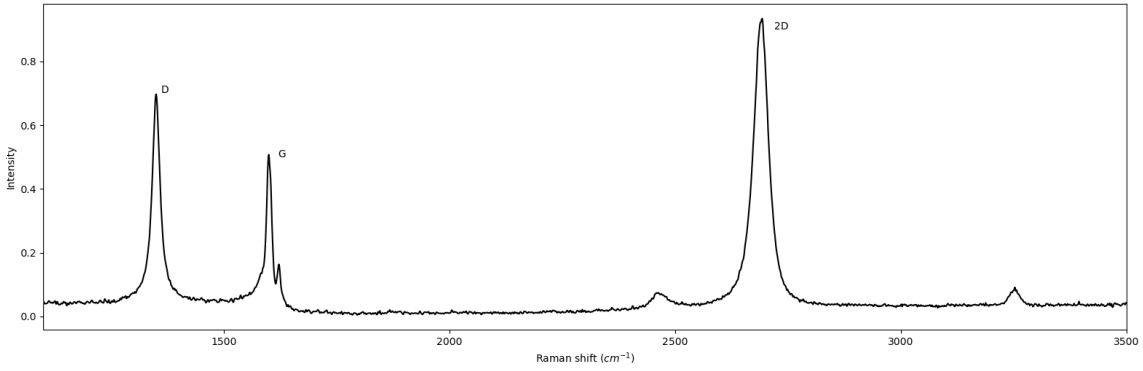

Figure 7. Raman spectrum of defected graphene, where the D peak is clearly visible. The spectrum has only a few prominent features, but it gives a lot of information about graphene's properties.

The ratio of the intensities of the D and G peaks I(D)/I(G) is often used as a measure of the disorder in graphene. The Raman response to disorder in graphite can be divided into three stages 1) graphite to nanocrystalline graphite 2) nanocrystalline graphite to amorphous carbon with low sp^3 content and 3) amorphous carbon with low to high sp^3 content [42]. This classification is also applicable to graphene. In the lowest disorder stage the intensity of the D peak increases, all peaks broaden and the D' peak appears at 1620 cm^{-1}. As the peaks broaden the nearby G and D' peak can appear to be a single upshifted G peak. In the second disorder range the intensity of the D peak decreases as the sp^2 rings whose breathing modes it originates from decrease, the G peak shifts back down and the second order peaks flatten out. The third, high disorder regime is not necessarily relevant to the study of graphene, but its main feature is the increase in the G peak position.

3.2 Atomic force microscopy

Atomic force microscopy is a type of scanning electron probe microscopy, which is a branch of microscopy, where the image is formed using a physical probe. AFM is a high-resolution imaging method, that can be used to map the topology of a samples surface. Besides its high resolution, AFM has the advantage of not needing a conductive sample or a vacuum. It is best suited for imaging small areas, as the imaging time is dependent on the image size and quality.

An atomic force microscope produces an image by going over the sample surface

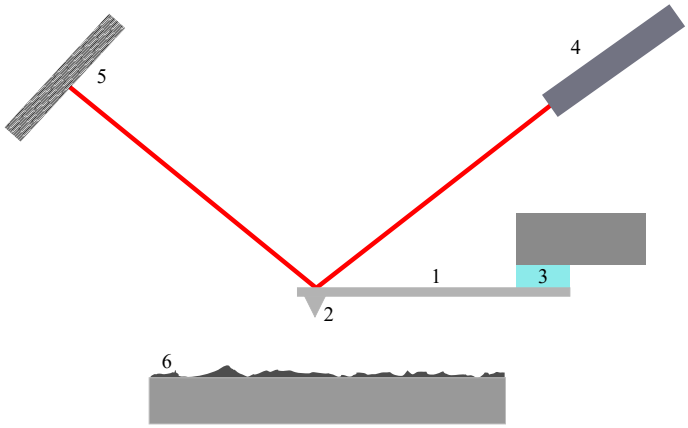

Figure 8. Schematic of the atomic force microscope. The basic components of the AFM are 1) the cantilever, 2) the cantilever tip, 3) the piezoelectric element, 4) laser, 5) photodiode detector and 6) the sample.

with a physical probe, a cantilever with a small tip [43]. The motion of the cantilever is controlled with a piezoelectric element and the vertical movement of the probe is measured by reflecting a laser beam from the top of the probe to a position sensitive photodiode detector. The image is usually formed by deploying a feedback loop: the information on the movement of the probe from the photodiode detector is fed into the loop which controls the piezo to keep a set parameter e.g. the cantilever deflection at a constant, the resulting piezo movements thus following the topology of the sample, forming the image. The general composition an atomic force microscope is presented in figure 8. An AFM can be operated in three distinct modes, contact, non-contact and tapping, that produce the image in differing ways.

The simplest of the AFM operating modes is contact mode. In contact mode atomic force microscopy, the tip is scanned, line by line, along the sample surface. In contact mode the monitored signal is the deflection of the cantilever, and its height is continually adjusted via the feedback loop to keep the deflection, and thus the force between the sample and the tip, constant. Contact mode has the drawback of applying relatively large lateral forces to the sample, which can damage the sample and the cantilever tip.

In non-contact mode the cantilever is oscillated near the sample surface, but not touching it. The changes in either the amplitude or the resonant frequency are mapped. Like in contact mode, a feedback loop is used to keep the frequency or amplitude constant as the interaction between the tip and the sample affects them [44]. Non-contact mode prevents cantilever tip degradation, as it eliminates the lateral forces present in contact mode.

In tapping mode, the cantilever is oscillated close to its resonance frequency near the sample, so that at the lowest point it comes into contact, or "taps", the sample surface. A feedback loop is used to keep the amplitude of the oscillation constant as the short range repulsive and long range attractive interactions affect the amplitude close to the sample [44]. Tapping mode has the advantage of better preserving tip quality and the sample during imaging, while still producing images with high lateral resolution.

The AFM imaging mode utilised in this work was the peak force tapping mode. Unlike the conventional tapping mode, in the peak force tapping mode the cantilever is oscillated well below the resonance frequency. As the name implies, in peak force tapping mode the peak interaction force, obtained from the measured cantilever

deflection, is kept constant with a feedback loop [45]. Peak force tapping mode has the advantage of combining the direct force control of contact mode with the lessened lateral forces of tapping mode.

4 Experimental methods

4.1 Sample preparation

The samples studied in this thesis were prepared by Olli Rissanen. The graphene was synthesised by CVD on copper, from where it was transferred to a silicon dioxide substrate using a PMMA support layer and annealed using a two-step process after the transfer. First the samples were annealed in a mixture of argon and hydrogen to break down the polymer residues, which results in the formation of amorphous carbon. After the first annealing round the samples are annealed again in oxygen to remove the amorphous carbon. The studied graphene hall bar devices with metal contacts for electrical measurements were fabricated from this graphene. The channel width of studied hall bars was 3 μm. The metal electrodes of the samples were connected to the chip carrier by gold wire bonded with a supersonic bonder.

4.2 Electrical measurements

The initial measurements on the samples were done before cleaning with THF, both in ambient conditions and in a glovebox with an argon atmosphere. The same measurements were repeated in argon after cleaning the samples with THF. The studied devices were chosen by first measuring device response to varying the bias voltage, discarding devices with lost contacts. The gate response of the devices was determined by first raising the bias voltage over the device to a constant of 1 V, after which, the gate voltage was varied between -30 V to 30 V. The measurements were controlled, and the results logged with a LabView program connected to a National Instruments data acquisition device (NIcDAQ 9174). The bias voltage was applied with a Keithley 2440 SourceMeter and the gate voltage with the NI9269 voltage output module of the DAQ. The voltages Vxx and Vxy in figure 9 measured over the hall bar legs were both passed through Dl Instruments 1201 voltage preamplifiers to get the resulting voltage range between -10 to 10 volts, the input range of the NI9239 voltage input module of the DAQ. The drain current was similarly passed through a DI Instruments current amplifier to achieve an output in that same voltage range.

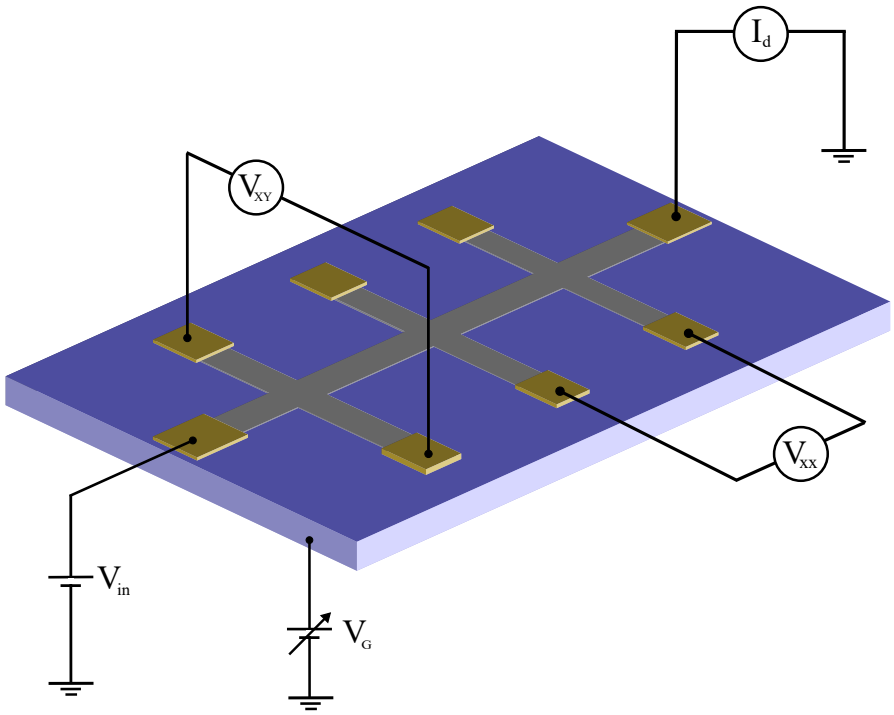

Figure 9. Schematic of the gated graphene hall bar device and an example of a circuit diagram for the gate sweep measurements.

All of the measurements were done using a four terminal setup to eliminate the effect of contact resistance. The circuit diagram for the gate sweep measurements is presented in figure 9, the circuit diagram for the bias sweep measurements differs from it only in that the input voltage Vin is variable, and no gate voltage is applied.

4.3 Graphene quality and topology measurements

AFM imaging was used to estimate the intactness of the devices and the amount of residues on the sample, verifying the starting point before THF cleaning and mapping the results after. The AFM imaging was done with the Bruker Dimension Icon AFM, using the PeakForce Quantitative Nanomechanical Mapping in air mode. ScanAsyst Air probes from Bruker were used for imaging, with the peak force limited to 2 nN.

The quality of the graphene and the amount of doping were estimated using Raman spectroscopy. The Raman spectroscopy was done using the Nicolet DXR

Raman spectroscope using a 532 nm excitation wavelength, using a laser power of 0.5-1 mW. The measurement time per accumulation was 10 s. Like the AFM imaging the Raman spectroscopy measurements were repeated after cleaning the samples to estimate the effectiveness of THF cleaning for removing PMMA residues and surface doping from graphene.

4.4 THF cleaning

The graphene samples were transferred into an argon atmosphere before cleaning to avoid immediate re-contamination from ambient sources. The cleaning process consisted of pipetting a drop of dry THF onto the sample surface, waiting 60 seconds, and then carefully blowing the THF droplet away from the sample surface with an argon gun. Despite its apparent simplicity, this process requires careful precision. It is necessary to ensure that before it is blown away, the THF never spreads out from the top of the sample into the chip holder, because this can cause the flushing of additional contaminants onto the sample surface. When blowing the THF droplet away, one should also be careful to blow the argon onto the sample directly down from above the center of the sample, not from the side, since this can cause the contaminants to just move around on the sample surface.

5 Experimental results

5.1 Electrical measurements

5.1.1 Effect of THF cleaning

The results of electrical measurements for three of the studied graphene devices, referred to here as devices A, B and C, are presented in this section. Out of the studied devices A and B are parts of the same Hall bar. The intactness and quality of these devices was verified as described in chapter 4. The devices are on the same chip, fabricated from the same graphene sheet. Because of this, their characteristics can be expected to be relatively similar when ignoring factors such as large wrinkles in the graphene or considerable inhomogeneities in the PMMA residues.

The dependences of the drain current I_d on the drain voltage V_d for the devices were measured first in air, then in a glovebox environment in argon and finally in argon after cleaning them with THF. The results are presented in figure 10. With a constant (zero) gate voltage ordinary graphene behaves like a resistor, and all three devices presented linear I-V characteristics as expected. The resistances of the devices between the different measuring conditions behaved similarly for all three devices. The zero-gate resistances for all devices increased slightly when the sample was moved from air to argon and increased considerably after cleaning the samples with THF. Especially device A showed a large increase in resistance after THF cleaning.

Before THF cleaning the devices exhibited similar gate responses, shown in figure 11, the Dirac point for all three residing far to the right of the zero-gate voltage, somewhere above 30 volts. This indicates that the devices were highly p-type doped. The comparisons between the pre-cleaning gate sweep measurements done in air and in argon show a small shift in the Dirac peak position corresponding to a slight reduction in doping as the sample acclimates into the inert atmosphere. This is in agreement with the obtained zero-gate resistances. The difference is observable, but very small, and still leaves the Dirac peak well out of the reach of the used gate

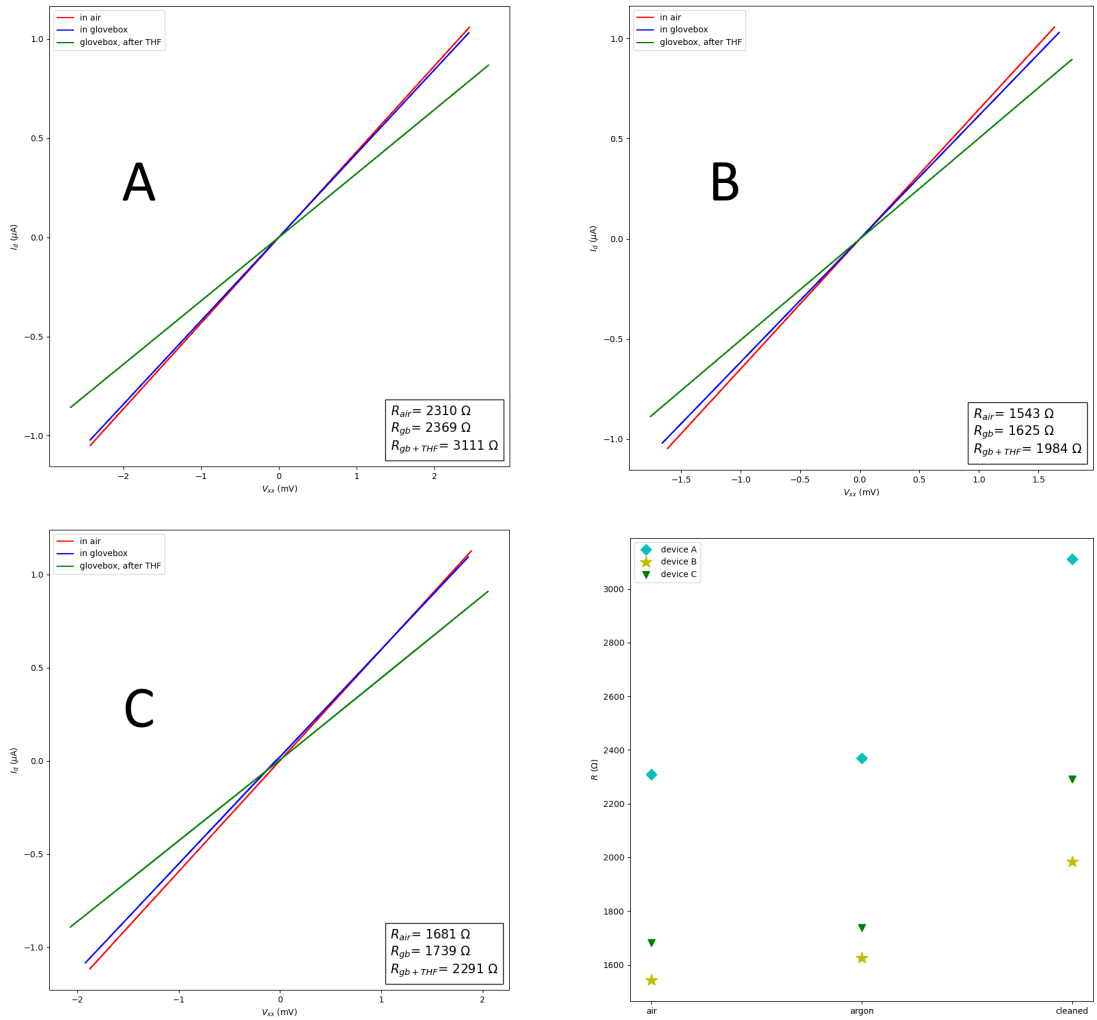

Figure 10. Drain current versus drain voltage in air, in argon and in argon after THF cleaning for devices A, B and C. The changes in resistance followed the same pattern across all devices.

voltage range.

The resistance versus gate voltage behaviour after the devices were cleaned with THF is shown in figure 11. Device C lost most contacts after cleaning, so the resistance-gate voltage behaviour is only presented for devices A and B. Compared to before cleaning, the Dirac peak has shifted far closer to the zero-gate voltage point, indicating removal of p-type doping. The resistance also exhibits hysteretic behaviour over the gate voltage sweep, showing a large shift in the Dirac peak position when the sweeping direction changes. Hysteresis in graphene devices is generally due to either charge transfer, that causes a positive shift in the gate voltage

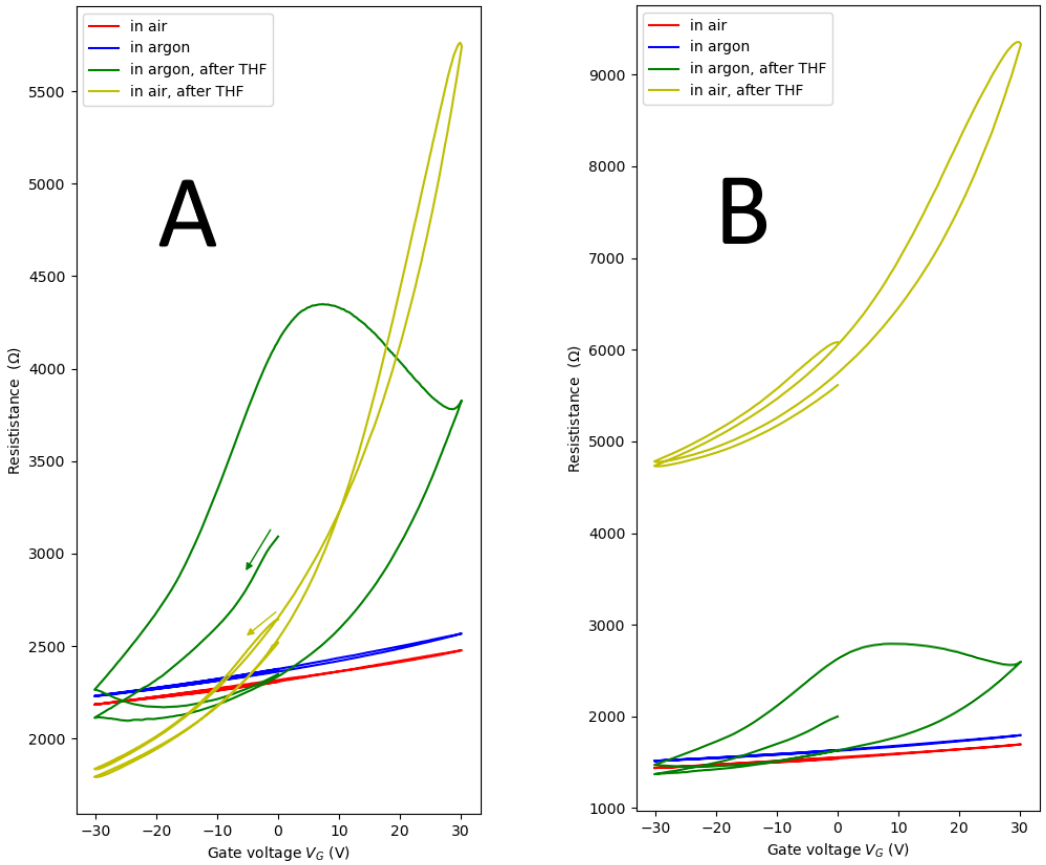

Figure 11. Resistance versus gate voltage before and after the THF cleaning for devices A and B. Before cleaning the graphene devices are p-doped, as the Dirac point is to the right of the zero-gate voltage. Gate voltage versus resistance after the sample was cleaned with THF show that the maximum resistance point has moved towards the zero gate voltage, meaning some doping has been successfully removed.

of the maximum resistance or capacitive gating that in turn causes a negative shift [46]. Due to the strong hysteresis, it is impossible to determine whether the Dirac point is actually reached during the gate sweep or if the maximum resistivity seen on the return gate sweep pass is seen because of a reduction in p-type doping caused by charge redistribution that is slower the sweeping rate. The observed hysteresis is unusually strong, similar hysteretic behaviour generally being reported only in graphene-heterostructures.

After the cleaned devices were exposed to air again, it can be seen that the resistance peak shifts back to the right but remains closer to the zero-gate voltage

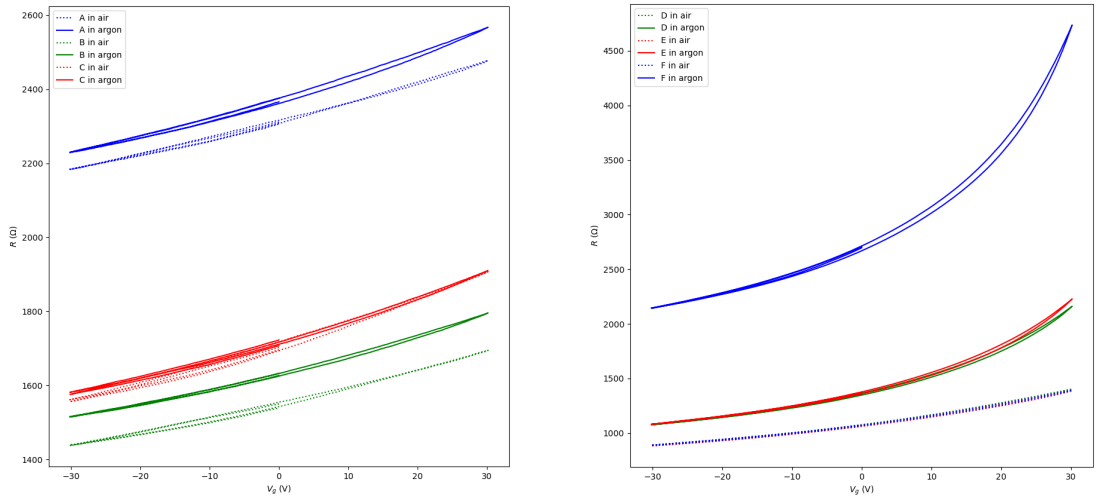

(a) **(b)**

Figure 12. The resistance versus gate voltage in air and in argon for **a)** devices A, B and C with higher amounts of PMMA residues and **b)** devices D, E and F with fewer PMMA residues.

than before cleaning. For device B a large increase in overall resistance is also observed. The four terminal measurement setup eliminates increased contact resistance as a possible source, but another possible cause for the increased resistance could be the degradation of the sample. The hysteresis effect observed after the cleaning in argon is strongly suppressed. After exposing the devices to air, it can be assumed that the resulting difference in device behaviour is a result of re-accumulating ambient contamination. Thus, the difference between the measurements done in air after THF and the initial measurements done in air could be assumed to be due to changes in the PMMA residues. Assuming PMMA-residues were the majority source of the p-type doping, this would indicate the successful removal of residues. However, the AFM images of the devices presented in section 5.2 clearly show large amounts of residues.

5.1.2 In air versus in argon

The effect of surrounding atmosphere was studied for two different samples and a total of six devices. The devices A, B and C are the same devices considered previously. Devices D, E and F are on another sample, that had fewer PMMA residues. The measured resistance versus gate voltage behaviour for the samples is presented in figure 12. When moved from air to argon, the samples consistently

show a small improvement in the amount of doping for all devices, indicated by the Dirac peak shifting closer to the zero-gate voltage. Devices on the cleaner sample show close to identical gate responses in air and show a clear improvement when moved into argon, especially for device F, whereas the devices on the other sample show varying gate responses at the start and considerably smaller improvements when moving the sample into argon. The observed shift when the samples are moved into argon is most likely due to a reduction in ambient contamination, that as the samples are moved into an inert atmosphere. The smaller shifts for the sample with higher PMMA residue could be due to the p-type doping from PMMA being a larger part of the combined doping from PMMA residues and ambient contamination.

5.2 AFM images

The initial AFM images, presented in figure 13, show that the topology of the graphene is flat, with sub 5 nm variation arising from wrinkles on the graphene

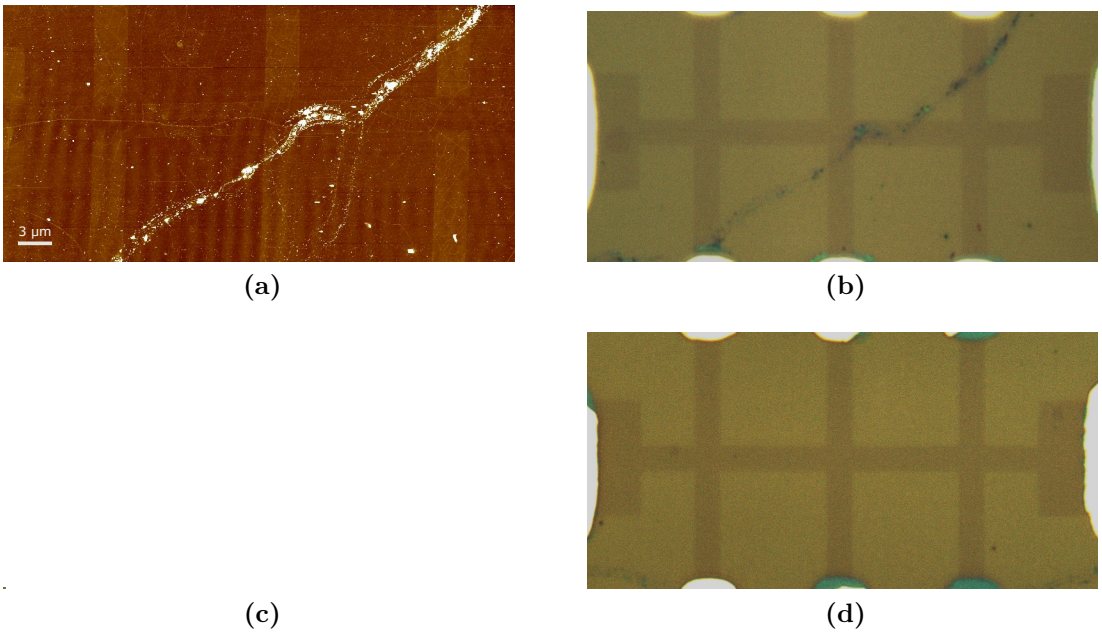

Figure 13. AFM **a)**,**c)** and optical images **b)**,**d)** of the studied devices before cleaning. In the initial AFM images PMMA residue from sample preparation is clearly visible as small higher dots on the sample surface. One of the studied Hall bars pictured in **a)** and **b)** shows large amounts of residues and large wrinkle in the graphene. The hallbar pictured in **c)** and **d)** shows a moderate amount of residues.

surface. The initial images also show clear PMMA residues on the graphene surface for all samples, seen as higher white dots in the image. The distribution of the PMMA residues is far from uniform and so is their effect on the graphene. Since the graphene was otherwise observed to be of relatively uniform quality, this could partly explain the large differences in the measured initial zero-gate resistances between the devices. The studied devices A and B correspond to the right and left sections from the center of the Hall bar presented in figure 13a respectively. The device C corresponds to the left of center part of the Hall bar presented in figure 13c.

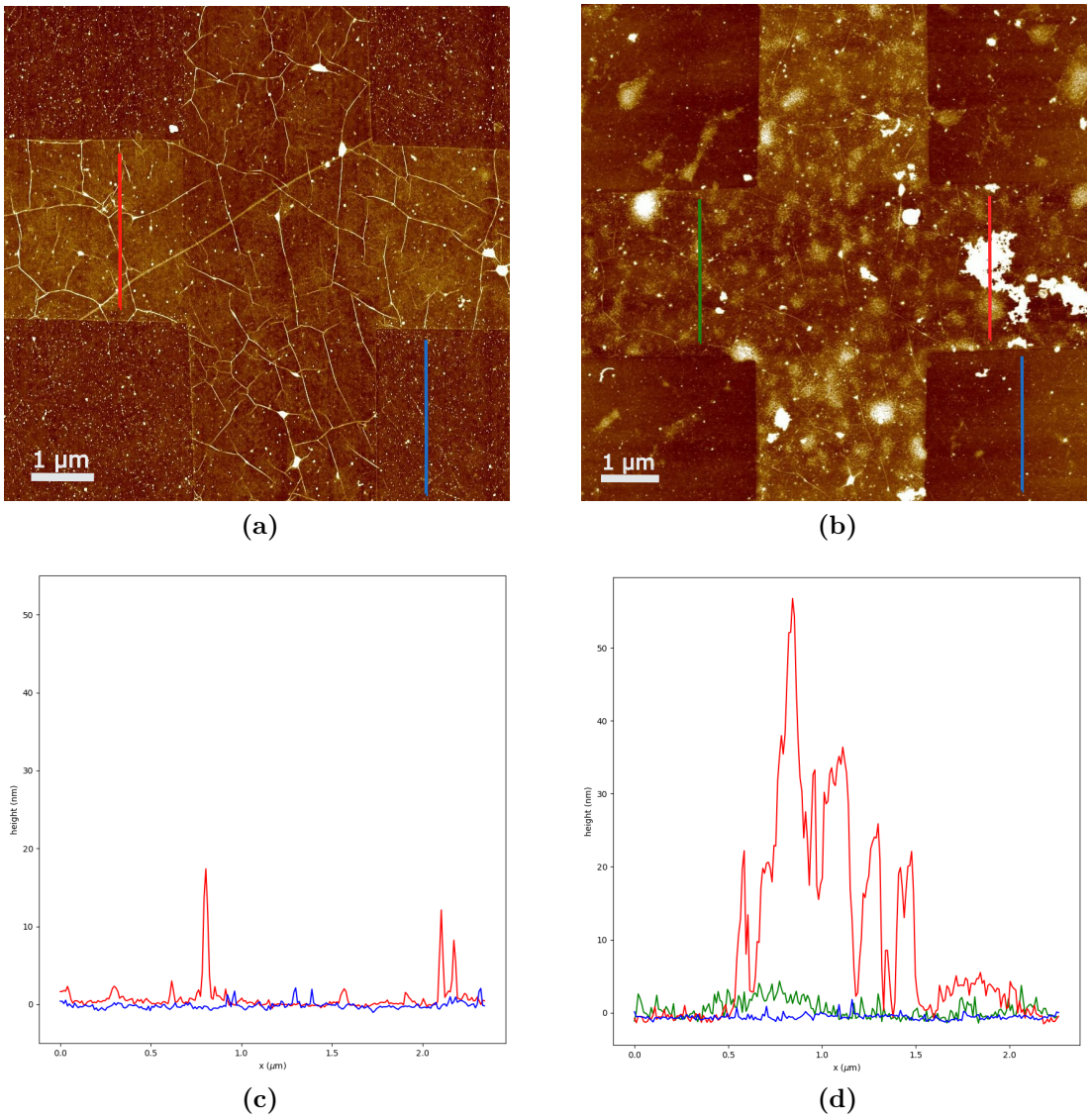

Figure 14. a) Close-up AFM image of the center of the Hall bar with device C before and **b)** after cleaning the sample with THF.

After the THF cleaning we can observe new residues on the graphene surface as shown in figure 14. The new residues are on average larger in size than the majority of the PMMA residues seen in the AFM images taken before cleaning. Most of these residues are most likely redeposition of PMMA on the sample surface, since it can be seen in the initial AFM and optical images that there were large PMMA residue domains on multiple points on the sample and the overall amount of initial PMMA residues was larger than for other studied samples, as can be seen in figure 13.

As can be seen in figure 14, the types of residues on the sample surface can be roughly divided into two groups: 1) the sub 10 nm residues evenly distributed all over the sample an 2) the few large, at points over 50 nm tall, residues. The heights of the larger residues are consistent with the larger PMMA deposits seen in figure 13, but they could also originate from a different source, possibly from redeposition of metal particles lifted off from the electrodes during ultrasonic bonding.

Even disregarding the new residues, looking at figure 14 it can clearly be seen that most of the initial PMMA residues have been unaffected by the THF rinsing. The only noticeable difference in amount of residues seems to be on SiO2. This would indicate that either the used THF cleaning procedure is insufficient for removing PMMA residues to begin with or the cleaning effect diminishes greatly when there is a large amount of PMMA residue on the sample.

5.3 Raman spectra

Initial Raman spectroscopy shows that the graphene quality is relatively good, the lack of a visible D-peak indicating few defects and the narrow 2D peak shows that the graphene is single layer. The samples have some surface doping, as the G peak at 1602 cm^{-1} is notably upshifted compared to that of pristine graphene at around 1580 cm^{-1}. Based on the initial electrical measurements the doping can be assumed to be p-type. The 2D peak at 2698 cm^{-1} is close to that of pristine graphene at around 2700 cm^{-1}.

After THF cleaning there is a slight blueshift in both the G and 2D peaks. The G peak shifting down could indicate a decrease in surface doping. After the THF cleaning the G peak shifted from 1602 cm^{-1} to 1591 cm^{-1} and the 2D from 2698 cm^{-1} to 2685 cm^{-1}. The G peak downshift indicates a reduction in doping as does the 2D downshift. The G peak of graphene's Raman spectrum shifts up with doping regardless of its nature, so it can only be used to assess the amount of doping,

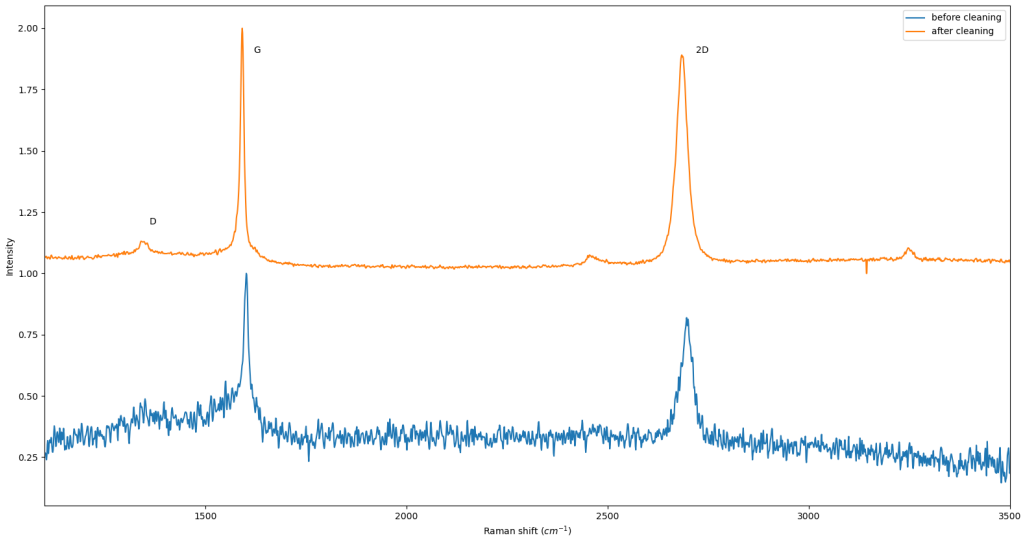

(a)

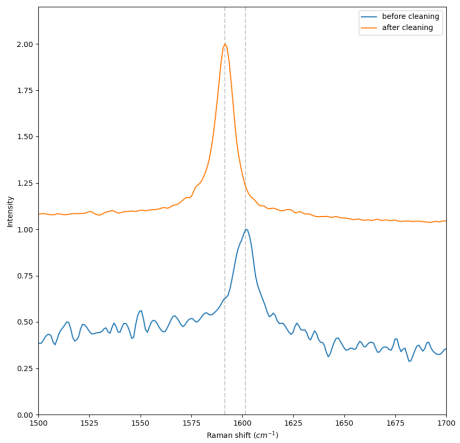

(b)

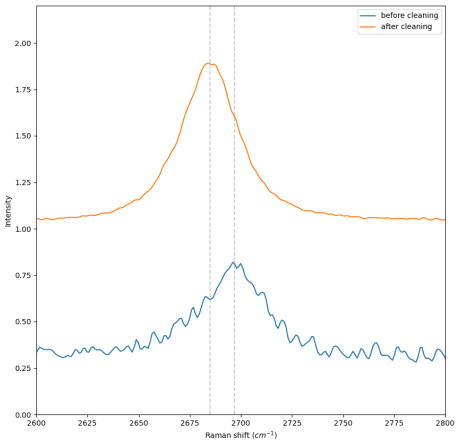

(c)

Figure 15. **a)**The Raman spectra before and after cleaning the sample with THF.**b)** close-up of the G-peak and **c)** 2D-peak

whereas the 2D peak behaves differently with for of hole and electron type doping. In this case the 2D peak shifting down indicates a reduction in p-type doping [41].

5.4 Suitability of THF for graphene cleaning

THF was unsuited to be used in tandem with the silver paste used to adhere the gate to the wiring connecting to the chip carrier. The THF dissolved the silver paste, resulting in multiple lost samples, both because of the lost gate contact and thanks to the surface of the sample becoming contaminated by silver particles. This was amended in following samples by wirebonding the gate connection instead. While THF shows some promise for removing both PMMA residue and surface doping, it leaves a lot to be desired. Cleaning the samples with THF often produced varying results, despite the cleaning process remaining practically unchanged. In some cases, THF cleaning left a film on the sample surface, largely defeating its purpose of removing contaminants from the graphene. However, these films only appeared because of issues in the cleaning process, likely because of the THF drying before being blown away with argon during one of the cleaning steps. In a few samples some graphene was lost during cleaning, but this was rare and likely caused by poor adhesion of the graphene to the substrate.

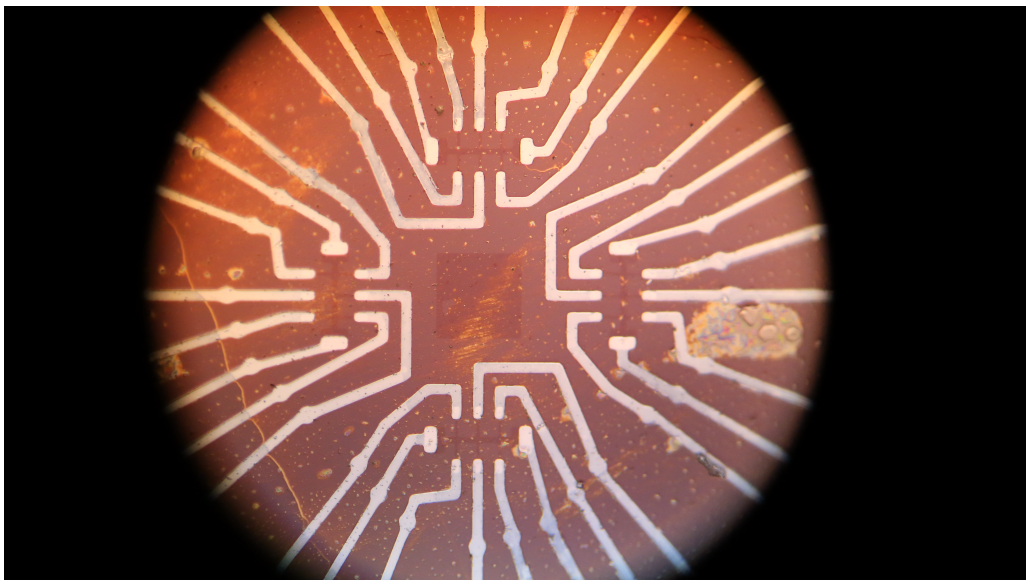

Figure 16. Optical microscope image of a sample contaminated by particles from the silver paste detached by THF.

6 Conclusions

The work and results presented in this thesis for THF cleaning of PMMA residues from graphene can aid in the improvement of the graphene transfer process and act as a starting point for further research into the THF cleaning of graphene. While the expected results for THF cleaning were not achieved in this work, the used cleaning method with the studied samples showed promise for removing surface doping from ambient sources. The THF rinsing was not found to have any notable effect on the amount of PMMA residues on the sample surface. This, however, should not be taken as proof of its unsuitability for cleaning PMMA residue from graphene, but rather as an example of some of the many factors that can affect the THF cleaning process. The two most considerable factors recognised in this work were: 1) using THF cleaning on samples that had silver paste in the gate-chip carrier connection, can render samples instantly unserviceable, due to silver particles drifting to the sample surface and 2) considerable amounts of PMMA residue on the sample can weaken the effect of THF cleaning and lead to redistribution of PMMA on the sample surface. The former can now be avoided by metallizing gate electrodes on to the sample and connecting them to the chip carrier via ultrasonic bonding. The latter merits further study, as the hinderance to the THF cleaning effect was surprisingly large, and the exact cause of the failure could not be determined based on the work done for this thesis. Disregarding the PMMA residue removal, the clear success of removing ambient surface doping is a promising result. Even as more robust cleaning methods produce better overall cleaning results, convenient methods, such as solvent rinsing for removing surface doping are just as needed.

Even as THF cleaning failed in the specific cases presented in this work, it merits further study. THF is mentioned as a recognised efficient solvent for PMMA in many articles, but there remains a distinct lack of published work focusing on THF cleaning for removing PMMA residues from graphene. To better understand THF cleaning and to allow for clearer comparisons between it and other cleaning methods, methodical study of the different parameters affecting THF cleaning is needed. Further studies could employ the same means used to study other cleaning

methods, such as using deuterated PMMA to allow for closer monitoring of PMMA residues [11] or using x-ray photoelectron spectroscopy [16] or neutron reflection [47] to assess the amount and form of PMMA residues .

References

[1] K. Novoselov ym. “2D materials and van der Waals heterostructures”. In: *Science* 353.6298 (2016). DOI: 10.1126/science.aac9439.

[2] “Recent Advances in Ultrathin Two-Dimensional Nanomaterials”. In: *Chemical Reviews* 117 (9 May 2017), pp. 6225–6331. ISSN: 15206890. DOI: 10.1021/acs.chemrev.6b00558.

[3] K. Novoselov ym. “Electric field in atomically thin carbon films”. In: *Science* 306.5696 (2004), pp. 666–669. DOI: 10.1126/science.1102896.

[4] C. Lee ym. “Measurement of the elastic properties and intrinsic strength of monolayer graphene”. In: *Science* 321.5887 (2008), pp. 385–388. DOI: 10.1126/science.1157996.

[5] H. Chen ym. “Mechanically strong, electrically conductive, and biocompatible graphene paper”. In: *Advanced Materials* 20.18 (2008), pp. 3557–3561. DOI: 10.1002/adma.200800757.

[6] Y. Wu ym. “State-of-the-art graphene high-frequency electronics”. In: *Nano Letters* 12.6 (2012), pp. 3062–3067. DOI: 10.1021/nl300904k.

[7] S. P. Lonkar, Y. S. Deshmukh, and A. A. Abdala. “Recent advances in chemical modifications of graphene”. In: *Nano Research* 8.4 (2015), pp. 1039–1074. DOI: 10.1007/s12274-014-0622-9.

[8] F. Liu and Z. Fan. “Defect engineering of two-dimensional materials for advanced energy conversion and storage”. In: *Chemical Society Reviews* 52.5 (2023), pp. 1723–1772. DOI: 10.1039/d2cs00931e.

[9] F. Guinea, M. Katsnelson, and A. Geim. “Energy gaps and a zero-field quantum hall effect in graphene by strain engineering”. In: *Nature Physics* 6.1 (2010), pp. 30–33. DOI: 10.1038/nphys1420.

[10] A. Johansson ym. “Optical Forging of Graphene into Three-Dimensional Shapes”. In: *Nano Letters* 17.10 (2017), pp. 6469–6474. DOI: 10.1021/acs.nanolett.7b03530.

[11] L. Lin ym. “Towards super-clean graphene”. In: *Nature Communications* 10.1 (2019). DOI: 10.1038/s41467-019-09565-4.

[12] Y. Zhang, L. Zhang, and C. Zhou. “Review of chemical vapor deposition of graphene and related applications”. In: *Accounts of Chemical Research* 46.10 (2013), pp. 2329–2339. DOI: 10.1021/ar300203n.

[13] M. S. A. Bhuyan ym. “Synthesis of graphene”. In: *International Nano Letters* 6.2 (2016), pp. 65–83. DOI: 10.1007/s40089-015-0176-1.

[14] Q. Yu ym. “Graphene segregated on Ni surfaces and transferred to insulators”. In: *Applied Physics Letters* 93.11 (2008). DOI: 10.1063/1.2982585.

[15] A. Reina ym. “Large area, few-layer graphene films on arbitrary substrates by chemical vapor deposition”. In: *Nano Letters* 9.1 (2009), pp. 30–35. DOI: 10.1021/nl801827v.

[16] B. Zhuang ym. “Ways to eliminate PMMA residues on graphene —— superclean graphene”. In: *Carbon* 173 (2021), pp. 609–636. DOI: 10.1016/j.carbon.2020.11.047.

[17] P. Wallace. “The band theory of graphite”. In: *Physical Review* 71.9 (1947), pp. 622–634. DOI: 10.1103/PhysRev.71.622.

[18] A. H. C. Neto ym. “The electronic properties of graphene”. In: *Reviews of Modern Physics* 81 (1 Jan. 2009), pp. 109–162. ISSN: 00346861. DOI: 10.1103/RevModPhys.81.109.

[19] N. Peres, F. Guinea, and A. Castro Neto. “Electronic properties of disordered two-dimensional carbon”. In: *Physical Review B - Condensed Matter and Materials Physics* 73.12 (2006). DOI: 10.1103/PhysRevB.73.125411.

[20] J.-H. Chen ym. “Intrinsic and extrinsic performance limits of graphene devices on SiO 2”. In: *Nature Nanotechnology* 3.4 (2008), pp. 206–209. DOI: 10.1038/nnano.2008.58.

[21] K. Bolotin ym. “Ultrahigh electron mobility in suspended graphene”. In: *Solid State Communications* 146.9-10 (2008), pp. 351–355. DOI: 10.1016/j.ssc.2008.02.024.

[22] X. Li ym. “Large-area synthesis of high-quality and uniform graphene films on copper foils”. In: *Science* 324.5932 (2009), pp. 1312–1314. DOI: 10.1126/science.1171245.

[23] A. Pirkle ym. “The effect of chemical residues on the physical and electrical properties of chemical vapor deposited graphene transferred to SiO2”. In: *Applied Physics Letters* 99.12 (2011). DOI: 10.1063/1.3643444.

[24] X. Yang and M. Yan. “Removing contaminants from transferred CVD graphene”. In: *Nano Research* 13.3 (2020), pp. 599–610. DOI: 10.1007/s12274-020-2671-6.

[25] M. Kim ym. “Direct transfer of Wafer-scale graphene films”. In: *2D Materials* 4.3 (2017). DOI: 10.1088/2053-1583/aa780d.

[26] T. Nasir ym. “Design of softened polystyrene for crack- and contamination-free large-area graphene transfer”. In: *Nanoscale* 10.46 (2018), pp. 21865–21870. DOI: 10.1039/c8nr05611k.

[27] W. S. Leong ym. “Paraffin-enabled graphene transfer”. In: *Nature Communications* 10.1 (2019). DOI: 10.1038/s41467-019-08813-x.

[28] Z. Zhang ym. “Rosin-enabled ultraclean and damage-free transfer of graphene for large-area flexible organic light-emitting diodes”. In: *Nature Communications* 8 (2017). DOI: 10.1038/ncomms14560.

[29] T. Wehling ym. “Molecular doping of graphene”. In: *Nano Letters* 8.1 (2008), pp. 173–177. DOI: 10.1021/nl072364w.

[30] H. Pinto and A. Markevich. “Electronic and electrochemical doping of graphene by surface adsorbates”. In: *Beilstein Journal of Nanotechnology* 5.1 (2014), pp. 1842–1848. DOI: 10.3762/bjnano.5.195.

[31] C. Melios ym. “Water on graphene: Review of recent progress”. In: *2D Materials* 5.2 (2018). DOI: 10.1088/2053-1583/aa9ea9.

[32] F. Schedin ym. “Detection of individual gas molecules adsorbed on graphene”. In: *Nature Materials* 6.9 (2007), pp. 652–655. DOI: 10.1038/nmat1967.

[33] J. Zhang ym. “Large-Area Synthesis of Superclean Graphene via Selective Etching of Amorphous Carbon with Carbon Dioxide”. In: *Angewandte Chemie - International Edition* 58.41 (2019), pp. 14446–14451. DOI: 10.1002/anie.201905672.

[34] Y.-C. Lin ym. “Graphene annealing: How clean can it be?” In: *Nano Letters* 12.1 (2012), pp. 414–419. DOI: 10.1021/nl203733r.

[35] A. Goossens ym. “Mechanical cleaning of graphene”. In: *Applied Physics Letters* 100.7 (2012). DOI: 10.1063/1.3685504.

[36] D. Ferrah ym. “XPS investigations of graphene surface cleaning using H2- and Cl2-based inductively coupled plasma”. In: *Surface and Interface Analysis* 48.7 (2016), pp. 451–455. DOI: 10.1002/sia.6010.

[37] Y. Dan ym. “Intrinsic response of graphene vapor sensors”. In: *Nano Letters* 9.4 (2009), pp. 1472–1475. DOI: 10.1021/nl8033637.

[38] A. C. Ferrari and D. M. Basko. “Raman spectroscopy as a versatile tool for studying the properties of graphene”. In: *Nature Nanotechnology* 8.4 (2013), pp. 235–246. DOI: 10.1038/nnano.2013.46.

[39] A. Ferrari ym. “Raman spectrum of graphene and graphene layers”. In: *Physical Review Letters* 97.18 (2006). DOI: 10.1103/PhysRevLett.97.187401.

[40] A. C. Ferrari. “Raman spectroscopy of graphene and graphite: Disorder, electron-phonon coupling, doping and nonadiabatic effects”. In: *Solid State Communications* 143.1-2 (2007), pp. 47–57. DOI: 10.1016/j.ssc.2007.03.052.

[41] A. Das ym. “Monitoring dopants by Raman scattering in an electrochemically top-gated graphene transistor”. In: *Nature Nanotechnology* 3.4 (2008), pp. 210–215. DOI: 10.1038/nnano.2008.67.

[42] A. Ferrari and J. Robertson. “Interpretation of Raman spectra of disordered and amorphous carbon”. In: *Physical Review B - Condensed Matter and Materials Physics* 61.20 (2000), pp. 14095–14107. DOI: 10.1103/PhysRevB.61.14095.

[43] G. Binnig, C. Quate, and C. Gerber. “Atomic force microscope”. In: *Physical Review Letters* 56.9 (1986), pp. 930–933. DOI: 10.1103/PhysRevLett.56.930.

[44] R. García and R. Pérez. “Dynamic atomic force microscopy methods”. In: *Surface Science Reports* 47.6-8 (2002), pp. 197–301. DOI: 10.1016/s0167-5729(02)00077-8.

[45] C. J. Shearer ym. “Accurate thickness measurement of graphene”. In: *Nanotechnology* 27.12 (2016). DOI: 10.1088/0957-4484/27/12/125704.

[46] H. Wang ym. “Hysteresis of electronic transport in graphene transistors”. In: *ACS Nano* 4.12 (2010), pp. 7221–7228. DOI: 10.1021/nn101950n.

[47] R. Li ym. “Determination of PMMA Residues on a Chemical-Vapor-Deposited Monolayer of Graphene by Neutron Reflection and Atomic Force Microscopy”. In: *Langmuir* 34.5 (2018), pp. 1827–1833. DOI: 10.1021/acs.langmuir.7b03117.